Journal of Power Sources 236 (2013) 207–214

Contents lists available at SciVerse ScienceDirect

Journal of Power Sources

journal homepage: www.elsevier.com/locate/jpowsour

N-Methyl-*N*-propylpiperidinium bis(trifluoromethanesulfonyl)imide-based organic electrolyte for high performance lithium–sulfur batteries

Lina Wang, Hye Ryung Byon*

Byon Initiative Research Unit (IRU), RIKEN Advanced Science Institute (ASI), 2-1 Hirosawa, Wako, Saitama 351-0198, Japan

HIGHLIGHTS

- ► Design of PP13-TFSI/DME electrolyte for Li–S batteries.
- ► Suppression of internal shuttling using PP13-TFSI/DME.
- ► Achievement of reliable performance of Li–S batteries with PP13-TFSI/DME.

GRAPHICAL ABSTRACT

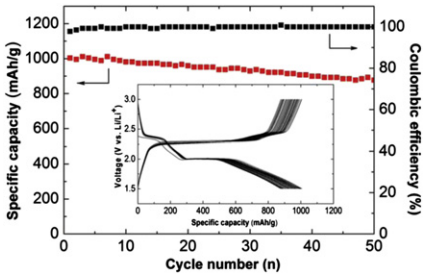

ARTICLE INFO

Article history:
Received 18 October 2012
Received in revised form
19 February 2013
Accepted 22 February 2013
Available online 4 March 2013

Keywords:
Energy storage
Lithium–sulfur battery
Ionic liquid
Electrolyte

ABSTRACT

Development of lithium–sulfur (Li–S) batteries has suffered from insufficient capacity and poor cycle-life. One of the reasons for these drawbacks is loss of active material, which is associated with the rapid diffusion of highly soluble lithium polysulfides formed as intermediates of discharge products in organic electrolytes, resulting in internal shuttling of lithium polysulfides. The diffusion of lithium polysulfides is determined largely by the physicochemical properties of electrolytes. Therefore, design of the physicochemical properties of the electrolyte to restrain the internal shuttling is vital to promote high performance for Li–S batteries. Here we present a newly designed room temperature ionic liquid (RTIL)-based organic electrolyte for Li–S battery. Our electrolyte provides a trade-off between solubility and diffusion rate of lithium polysulfides by mixing very different physicochemical properties of two solvents: high lithium polysulfide solubility of 1,2-dimethoxyethane (DME), and high viscosity of *N*-methyl-*N*-propylpiperidinium bis(trifluoromethanesulfonyl)imide (PP13-TFSI). An adequate composition ratio of mixed PP13-TFSI/DME afforded large capacity, high Coulombic efficiency, improved capacity retention, and suppressed internal shuttling.

1. Introduction

Rechargeable lithium–sulfur (Li–S) batteries have great potential as the next-generation of energy storage systems due to the high theoretical specific capacity (1675 mA h g^{-1}), low cost, and low environmental impact [1–3]. However, Li–S batteries have suffered from insufficient capacity and poor cycle-life due to the insulating nature of sulfur and discharge products (Li_2S_2 and Li_2S) as well as loss of active material by dissolution of lithium polysulfides (Li_2S_x, $4 \leq x \leq 8$) formed as intermediates of discharge products [1–10]. The endeavors for design of advanced cathode structures have mitigated these challenges [4–10]. Conductive micro/mesoporous carbon frameworks enable the efficient encapsulation of sulfur, with tunable pore size. The intimate contact between the conductive carbon framework and insulating sulfur at the nanometer scale is a plausible explanation for the observation

* Corresponding author. Tel.: +81 48 467 9265; fax: +81 48 462 1271.
E-mail address: hrbyon@riken.jp (H.R. Byon).

0378-7753/$ – see front matter © 2013 Elsevier B.V. All rights reserved.
http://dx.doi.org/10.1016/j.jpowsour.2013.02.068

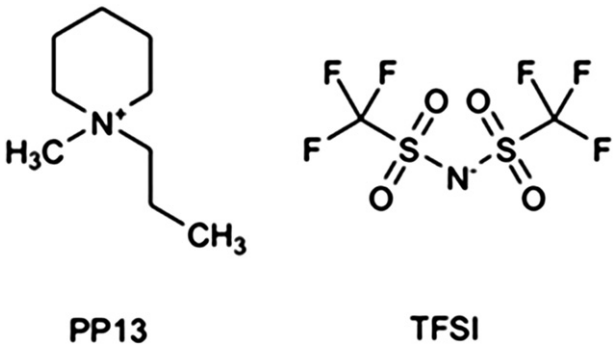

Fig. 1. The molecular structure of PP13-TFSI.

of reasonable electronic conductivity and utilization of active material, resulting in an enhanced capacity of over 1000 mA h g^{-1} for the initial cycle and good cyclability, of more than 50 cycles with over 90% Coulombic efficiency [4–10]. In addition, the development of silicon nanowire anodes [11] and gel polymer electrolytes [18] applied for Li–S batteries have also attempted to attain better performance. Nevertheless, Li–S batteries have still shown nontrivial overcharge and capacity fading around 35% decay after 10 cycles [1–3]. Therefore, ultimate solutions to resolve the challenges of Li–S batteries are still required.

The main issue of these drawbacks in Li–S batteries is associated with the rapid diffusion of highly soluble lithium polysulfides in organic electrolytes. An internal shuttle process of lithium polysulfides between cathode and anode causes loss of active material and degradation of the lithium anode through corrosion of the lithium surface by polysulfides, and subsequent production of a resistive precipitation-layer. Thus, a decrease of the lithium polysulfide diffusion rate can alleviate the current problems of Li–S batteries. The diffusion of lithium polysulfide is determined largely by the physicochemical properties of organic electrolytes [12–23]. Therefore, design of the physicochemical properties of the electrolyte to restrain the internal shuttle process is vital to promote high performance for Li–S batteries.

Nevertheless, thus far advances in the electrolyte for Li–S batteries have been limited. Promising single component organic solvents e.g., sulfone and tetra(ethylene glycol)dimethyl ether have been further developed by engineering of electrolyte composition in mixtures of organic solvents. Representatively, the mixture of 1,2-dimethoxyethane (DME)/1,3-dioxolane (DOL) (1/1, v/v) in the presence of lithium salt has been preferentially employed in attaining high specific capacity for the Li–S battery [4,7,8]. These ether-based electrolytes have high donor number and preferentially coordinate with Lewis acidic cation of Li^+. DME has high lithium polysulfide solubility and supplies a sufficient concentration of active material [15]. DOL also has a good polysulfide solubility and high stability for lithium anode as forming a passive solid-electrolyte interphase (SEI) layer on the lithium surface [17,21–23]. Consequently, this mixture can offer adequate specific capacity and cycle-life at high rate operation. However, DOL can be easily degraded by water, oxygen, and small amounts of

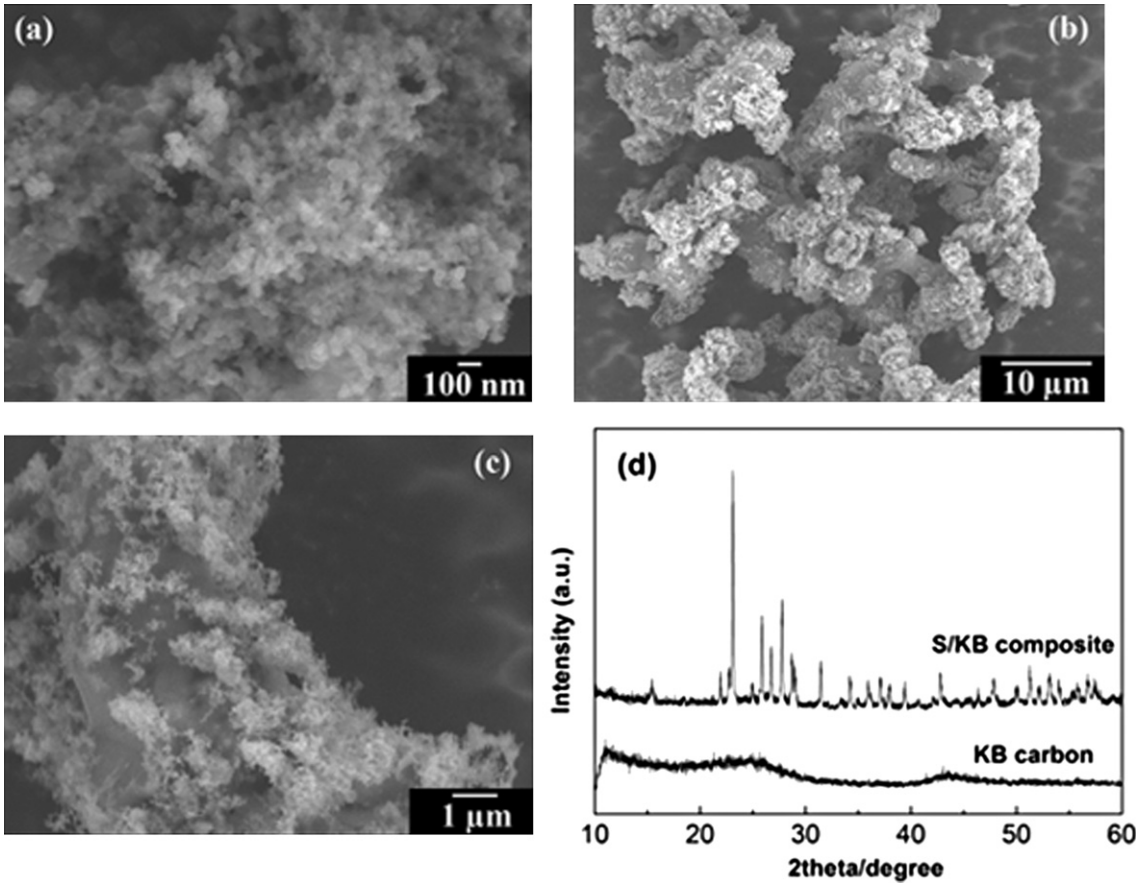

Fig. 2. Scanning electron microscopy (SEM) images of (a) pristine KB carbon, (b) low magnification, and (c) high magnification of S/KB composite. (d) X-ray diffraction (XRD) patterns of pristine KB carbon and as-prepared S/KB composite.

contaminants [22,23]. Furthermore, the inevitable self-discharge and internal shuttle can still occur at low current rate due to low viscosity of both solvents (0.46 and 0.6 cP at 25 °C for DME and DOL, respectively) [14].

Herein, we report a newly designed room temperature ionic liquid (RTIL)-based organic electrolyte by mixing DME and *N*-methyl-*N*-propylpiperidinium bis(trifluoromethanesulfonyl)imide (PP13-TFSI). A few studies reported RTIL-based organic electrolytes like imidazolium [13] or pyrrolidinium [19,20] RTILs with ether for Li–S batteries. These RTILs and ether combinations have shown the promising but moderate performance in terms of specific capacity and cycling stability. This is probably due to chemical inertia of the RTILs. Imidazolium-based ionic liquids, for example, was unstable with a lithium or graphite anode, which impeded the cyclic performance of Li–S batteries. The composition ratio of RTIL and ether also largely altered the physicochemical property of this mixture, thus affected solubility and diffusion rate of lithium polysulfides in Li–S batteries. We combined PP13-TFSI and DME in the optimum composition ratio, which achieved a trade-off between diffusion rate and solubility of lithium polysulfides. PP13-TFSI (Fig. 1) can offer a wide electrochemical window region (−0.3 V – 5.5 V vs. Li/Li$^+$) [24] for the Li–S electrochemical reaction. A feeble coordination of weak Lewis acid and base pairs like the typical aprotic RTILs alleviates lithium polysulfides solubility [15]. More importantly, extremely high viscous PP13-TFSI (117 cP at 25 °C) [24] relative to other RTILs is capable of suppressing lithium polysulfides diffusion rate noticeably. However, the use of PP13-TFSI only can provide a sluggish mass transport and charge transfer of lithium polysulfides in Li–S batteries, resulting in a low capacity. As combining PP13-TFSI with DME, two very different physicochemical characteristics can be counterbalanced as well as synergetically create the optimum condition for lithium polysulfide solubility and diffusion rate, which can afford large capacity, high Coulombic efficiency, improved capacity retention, and suppressed internal shuttling for Li–S battery.

2. Experimental

2.1. Preparation of S/KB electrodes

S was prepared according to the following chemical equation: $Na_2S_2O_3 + 2HCl \rightarrow 2NaCl + S(s) + H_2O + SO_2$. To prepare S/KB composite, 9.487 g of sodium thiosulfate ($Na_2S_2O_3$, 95%, Kanto Chemical) and 0.161 g of Ketjenblack (KB) carbon (ECP-600JD, received from AkzoNobel Polymer Chemicals) were mixed in 300 mL of deionized (DI) water (R = 18.2 MΩ) with vigorous stirring. 12 mL of aqueous hydrochloric acid (HCl, 35–37%, Wako Chemical) was then injected slowly into the mixture at 70 °C and vigorously stirred for 1 h. The S/KB composite was collected after cooling down to room temperature, washed thoroughly with DI water, and dried in a vacuum drier at 50 °C overnight. The S content in the S/KB composite was 90 wt% measured by thermogravimetric analysis (TGA, Seiko SSC/5200) under a nitrogen atmosphere. Additional KB powder was incorporated into the as-prepared S/KB composite with 60:40 mass ratio of S/KB:KB in *N*-methyl-2-pyrrolidone (NMP, 99.5%, Nacalai tesque) and mixed using a planetary mixer/deaerator (ARE-310, Thinky) at 2000 rpm for 10 min. The S/KB slurry was then cast on a glass fiber (GF/C, Whatman) and dried in a vacuum drier at 50 °C for at least 12 h for the evaporation of NMP. The completed S/KB electrode contained 54 wt% of S. For preparation of annealed S/KB electrode, the S/KB electrodes were heated at 155 °C for 3 h in a flow of argon gas at 20 mL min^{-1} to remove bare S in S/KB electrode.

2.2. Structural characterization

The surface morphology of S/KB composite was investigated using scanning electron microscopy (SEM, JEOL-6335). The X-ray diffraction (XRD) patterns were analyzed using Cu Kα of the radiation source at a voltage of 40 kV and a scan rate of 4° min^{-1} (RINT2000, Rigaku).

2.3. Preparation of electrolytes and Li–S cells

Lithium bis(trifluoromethanesulfonyl)imide (LiTFSI, LiN(CF_3SO_2)$_2$, >99.9%, Kishida Chemical) was dried in a vacuum drier before use. *N*-methyl-*N*-propylpiperidinium bis(trifluoromethanesulfonyl)imide (PP13-TFSI, Kishida Chemical) and 1,2-dimethoxyethane (DME, H_2O < 20 ppm, received from UBE) were mixed with 2/1 volume ratio containing 1 M of LiTFSI in an Ar-filled glove box (<1 ppm of H_2O and O_2, Kiyon). For the control experiments, we controlled volume ratio of PP13-TFSI/DME to 1/1. The single-solvent electrolytes, i.e., 1 M of LiTFSI with DME and 1 M of LiTFSI with PP13-TFSI were also prepared in a similar way.

All components used in the assembly of Li–S cells except the electrolytes and lithium metal were dried completely in a vacuum drier at 50 °C for 2 h before being transferred into the Ar-filled glove box to avoid possible contamination of water. Aluminum foil (as a current collector, d (diameter) = 16 mm), S/KB electrode on the

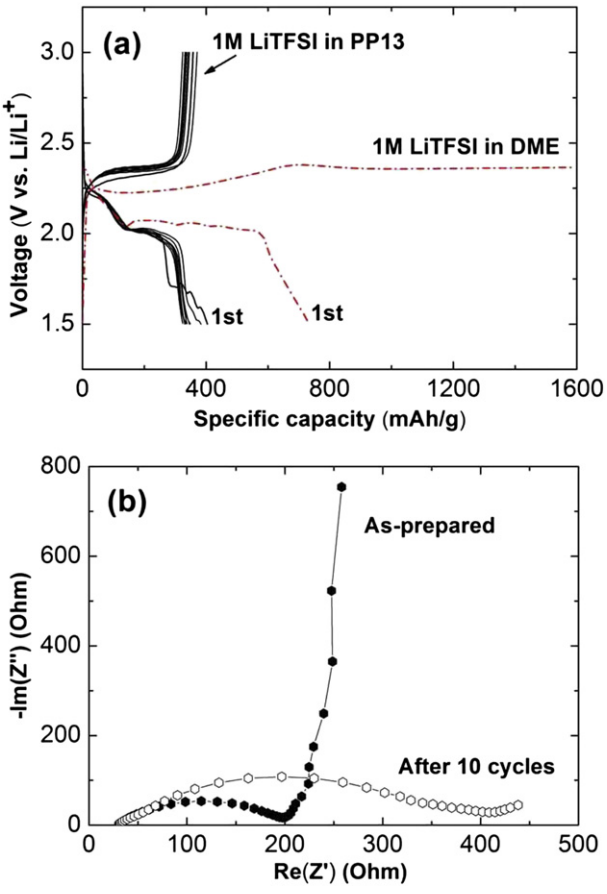

Fig. 3. Electrochemical performance of Li–S cells in single component solvents. (a) Discharge/charge profiles with 1 M of LiTFSI in DME (red dashed line of the first cycle) and in PP13-TFSI (black solid lines of 10 cycles) at 0.1 C (1 C = 1670 mA g^{-1}). (b) Electrochemical impedance spectra (EIS) as-prepared and after 10 cycles with 1 M of LiTFSI in PP13-TFSI electrolyte. (For interpretation of the references to color in this figure legend, the reader is referred to the web version of this article.)

glassy fiber (as a cathode substrate and separator, $d = 16$ mm), one piece of Celgard 2500 (as a separator, $d = 26$ mm, received from Celgard), and metallic lithium (Honjo) pressed on a stainless steel plate (as an anode, $d = 20$ mm) were sequentially assembled to two-electrode electrochemical cell (Tomcell®) with a total of 280 μL of electrolyte. The loading mass of S/KB was ~2 mg.

2.4. Electrochemical measurements

All electrochemical measurements were performed using a VMP3 battery testing system (Biologic Claix). Discharge/charge profiles were obtained in the voltage range of 1.5–3 V vs. Li/Li^+ at various current rates from 0.1 to 1 C (1 C = 1670 mA g^{-1}) with a galvanostatic mode. Electrochemical impedance spectroscopy (EIS) measurements were performed in the frequency range of 20 mHz–1 MHz at a potentiostatic signal amplitudes of 5 mV. The cyclic voltammograms (CVs) were measured in the voltage range of 1.5–3 V vs. Li/Li^+ at various sweeping rate from 0.01 to 1 mV s^{-1}. For open-circuit voltage (OCV) comparison, voltage changes from the assembled Li–S cells with different electrolytes were measured as a function of storage time before any electrochemical measurement.

3. Results and discussion

3.1. Structural and morphological characterization of S/KB electrodes

For examination of Li–S cell performance with respect to the electrolytes, we used a binder-free S/KB composite as the cathode. Small KB carbon nanoparticles were dispersed on large sulfur particles (~10 μm of diameter) as shown in the scanning electron microscopy (SEM) images (Fig. 2a–c), KB carbon has been shown to retain electronic conductivity and moderately impede active material loss via trapping of dissolved polysulfides [25]. The fabricated electrodes, containing ~54 wt% of sulfur, were shown to have an orthorhombic structure with respect to S in the X-ray diffraction (XRD) pattern, as shown in Fig. 2d. The diffraction of the S/KB composite shows two prominent peaks at $2\theta \approx 23^\circ$ and 28°, which is consistent with Fddd orthorhombic crystalline sulfur.

3.2. Electrochemical performance of Li–S cells using the single component electrolytes

The single component electrolytes (either DME or PP13-TFSI) with lithium salt allowed undesired parasitic reactions. Fig. 3a shows initial discharge/charge profiles of Li–S cells with 1 M of LiTFSI in DME and in PP13-TFSI at a current rate of 0.1 C (1 C = 1670 mA g^{-1}). Serious overcharge was observed with the DME-only electrolyte. Similarly, a single reduction peak and high oxidation baseline above 2.4 V vs. Li/Li^+ were observed in CV at a slow sweeping rate (0.01 mV s^{-1}, Fig. 4b). This reflects severe internal shuttling thus significantly reducing the Coulombic efficiency. We also found disappearance of higher-potential-reduction-peak (I_{pc1}) in this CV obtained after 10 scans of a fast sweeping rate (0.1 mV s^{-1}, Fig. 4a), of which CV presented obvious two reduction peaks (~2.4 and 2.0 V vs. Li/Li^+ for I_{pc1} and I_{pc2}, respectively) corresponding to sequential reductions (I_{pc1} to I_{pc2}) in the transformation of cyclo-octasulfur (S_8) to soluble lithium polysulfides (Li_2S_x, $4 \le x \le 8$) followed by formation of insoluble discharge products (Li_2S_2 and Li_2S).

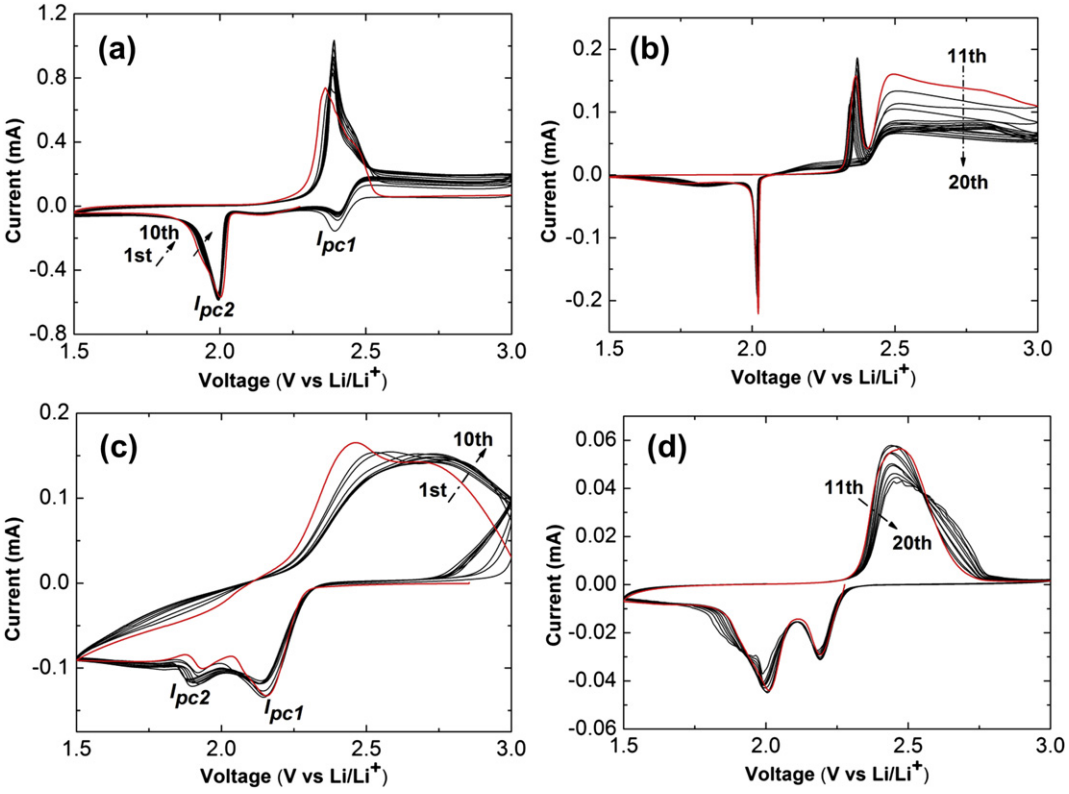

Fig. 4. Cyclic voltammogram (CV) curves of Li–S cells with 1 M of LiTFSI in DME and with 1 M of LiTFSI in PP13-TFSI. (a, c) The first 10 cycles at a sweeping rate of 0.1 mV s^{-1} with (a) 1 M of LiTFSI in DME and (c) PP13-TFSI, and (b, d) subsequent 10 cycles at 0.01 mV s^{-1} with (b) DME and (d) PP13-TFSI. The red lines indicate the initial cycle at the each sweeping rate. (For interpretation of the references to color in this figure legend, the reader is referred to the web version of this article.)

The discharge/charge profile with 1 M of LiTFSI in PP13-TFSI manifested three distinguished features compared with DME (Fig. 3a): a smaller value of initial discharge capacity (~405 mA h g^{-1}), no overcharge, and larger overpotential between discharge and charge plateaus. The small capacity and negligible overcharge are evidence of low utilization of active material and suppressed internal shuttling, respectively, which corresponds to slow diffusion rate of lithium-ion and polysulfides in PP13-TFSI. In addition, low lithium polysulfides solubility in PP13-TFSI can alleviate internal shuttling further. The huge polarization is attributed to extremely high viscosity of PP13-TFSI inducing large internal ohmic resistance and low ionic conductivity [15,26]. CV curves at a fast sweeping rate of 0.1 mV s^{-1} (Fig. 4c) exhibited broad reduction and oxidation peaks and gradually increased potential difference between reduction and oxidation peak upon cycling due to the electrolyte polarization effect. This polarization behavior, however, decreased at a slow rate of 0.01 mV s^{-1} (Fig. 4d). Discharge capacity values were quite stable for 10 cycles with PP13-TFSI-only electrolyte as shown in the discharge/charge profiles (Fig. 3a) while pronouncedly increased interfacial resistance was observed from electrochemical impedance spectra (EIS) in Fig. 3b. The interfacial resistance in the Nyquist plot, indicated by the intersection of semicircles with the real (Z) axis at lower frequency, is twice as large after 10 cycles compared with the as-prepared cell. Presumably, the RTIL with lithium polysulfides forms a resistive precipitation-layer on the lithium anode, which gradually corrodes the lithium anode on cycling [27].

3.3. Electrochemical performance of Li–S cells using PP13-TFSI/DME electrolytes

The combination of the two solvents with the optimum ratio of PP13-TFSI/DME (2/1, v/v) containing 1 M of LiTFSI prevented these parasitic reactions. The discharge/charge curves of Li–S cells upon the second cycle in PP13-TFSI/DME electrolyte are presented in Fig. 5 at current rates of 0.1, 0.2, 0.4, and 1 C. Two plateaus were displayed in both discharge/charge profiles, which was in agreement with the conspicuous reduction/oxidation peaks observed in the CVs (Fig. 6a and b). There is no evidence of polarization and internal shuttle process during cycles at both fast and slow sweeping rates. Furthermore, the Randles–Sevcik plot suggests that these redox reactions are diffusion controlled (Fig. 6c). The discharge capacity values at 0.1 C (~1360 and 1300 mA h g^{-1} for the first and the following cycle, respectively) were more than twice those observed with the 100% PP13-TFSI or 100% DME based electrolyte. At higher current rates, Li–S cells delivered lower capacities (~700 mA h g^{-1} at 0.2 and 0.4 C, and ~500 mA h g^{-1} at 1 C upon the second discharge) but afforded less capacity fading (~0.5% of averaged capacity fading per cycle at 0.2 and 0.4 C, and ~0.3% at 1 C from 2nd to 50th cycles) than the ones at 0.1 C (~1.7% of averaged capacity fading per cycle from 2nd to 15th cycles) (Fig. 7a). It implies that the internal shuttle process is inevitably incorporated in Li–S battery chemistry with PP13-TFSI/DME electrolyte while it is very gentle and further suppressed at

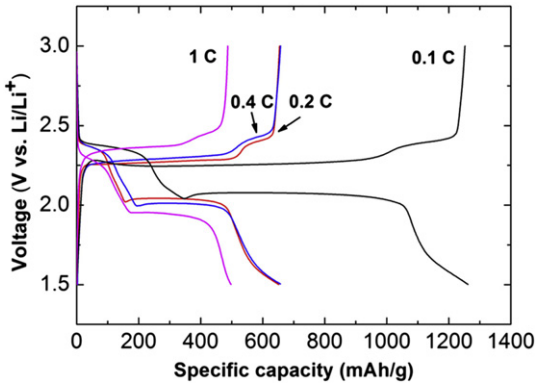

Fig. 5. The second cycle of discharge/charge profiles of Li–S cells with 1 M of LiTFSI in PP13-TFSI/DME (2/1, v/v) at current rates of 0.1, 0.2, 0.4, and 1 C.

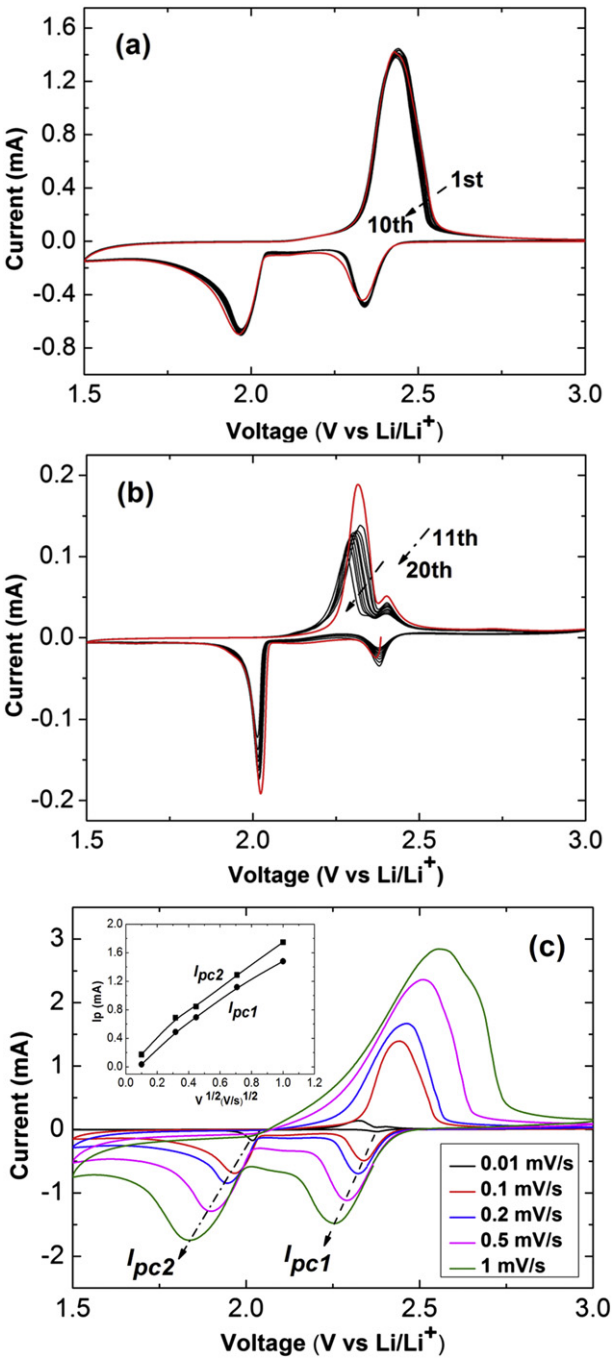

Fig. 6. CV curves of Li–S cells with 1 M of LiTFSI in PP13-TFSI/DME (2/1, v/v). (a) The first 10 cycles at a sweeping rate of 0.1 mV s^{-1} and (b) subsequent 10 cycles at 0.01 mV s^{-1}. The red lines in (a) and (b) indicate the initial cycle at the each sweeping rate. (c) Various sweeping rates from 0.01 to 1 mV s^{-1}. The inset in (c) reveals the Randles–Sevcik plot of the reduction peak currents (I_{pc1} and I_{pc2}) correlated with the square root of sweeping rate ($V^{1/2}$). (For interpretation of the references to color in this figure legend, the reader is referred to the web version of this article.)

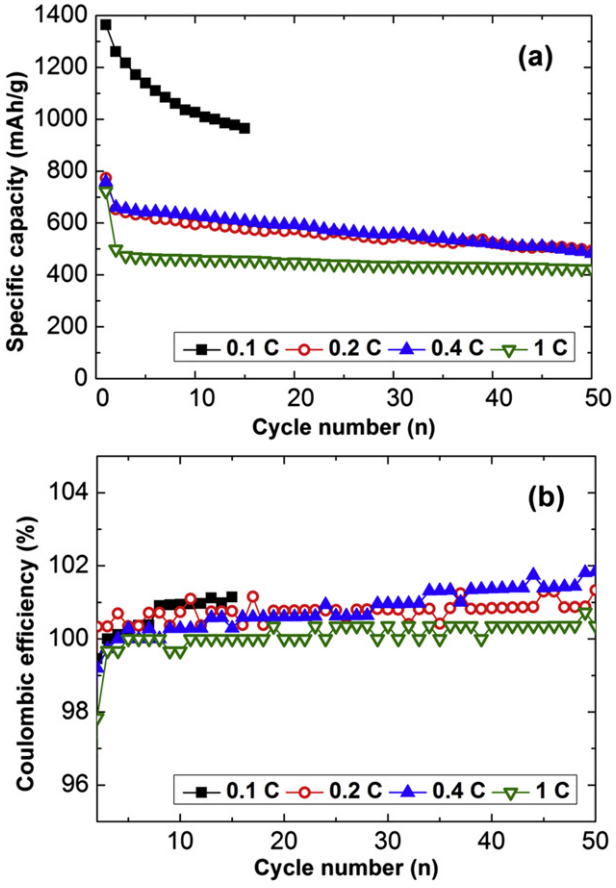

Fig. 7. Electrochemical performance of Li–S cells with 1 M of LiTFSI in PP13-TFSI/DME (2/1, v/v) at various current rates. (a) Cyclic performance and (b) Coulombic efficiency up to 50 cycles at 0.1–1 C.

higher current rates. This is consistent with the overcharge behavior approaching ~100% Coulombic efficiency and stable capacity retention toward higher current rates (Fig. 7b). The poor capacity retention at 0.1 C is attributed to the cumulative loss of active material. PP13-TFSI in PP13-TFSI/DME can suppress the lithium polysulfide diffusion rate but its effect can weaken at slower current rate due to an offer of abundant mass transportation and charge transfer chances. Nevertheless, we note again that the internal shuttling was efficiently suppressed and this is strong evidence for adequate solubilities and diffusion rates of lithium polysulfides in PP13-TFSI/DME electrolyte. A larger volume ratio of DME in PP13-TFSI/DME, for example, revealed poor Coulombic efficiency for 50 cycles (Fig. 8). Strong overcharge behavior in 1/1 volume ratio of PP13-TFSI/DME electrolyte results from a relatively higher lithium polysulfide diffusion rate.

The interfacial resistance slightly decreased after 50 cycles at 0.4 C from the as-prepared cell using the optimum volumetric composition of PP13-TFSI/DME (Fig. 9). It is possibly due to the formation of an improved passive SEI layer on the lithium anode from PP13-TFSI/DME with lithium polysulfides [19]. In addition, insignificant polarization (Fig. 5) in comparison with the overpotentials from PP13-TFSI-only electrolyte at 0.1 C (Fig. 3a) results from suitable viscosity and higher ionic conductivity of electrolyte. It can be confirmed by smaller solution resistance from PP13-TFSI/DME (~3 Ω in Fig. 9), indicated by the intersection with the Z′ axis at the higher frequency, relative to that from PP13-TFSI single electrolyte (~32 Ω in Fig. 3b). Moreover, the evidence of

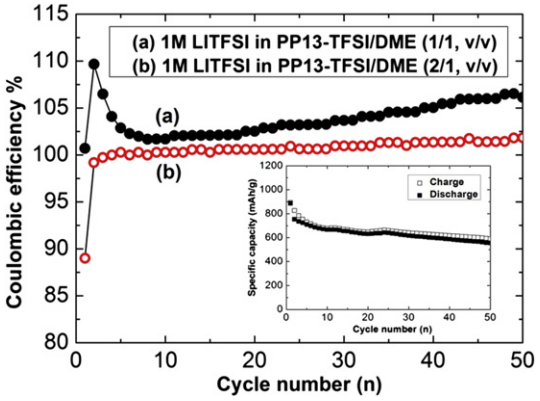

Fig. 8. Coulombic efficiencies of Li–S cells from different volume ratios of PP13-TFSI/DME (1/1 vs. 2/1). The inset is the capacity retention for 50 cycles at a current rate of 0.4 C with 1 M of LiTFSI in 1/1 volume ratio of PP13-TFSI/DME.

suppressed internal chemical shuttling in PP13-TFSI/DME could be attained by open-circuit voltage (OCV) correlated with time, from the as-prepared Li–S cells (Fig. 10). The initial OCVs of the Li–S cell using DME, PP13-TFSI, and PP13-TFSI/DME are 2.34 V, 2.78 V and 3.0 V respectively. PP13-TFSI/DME led to a gradual decrease in OCV reaching ~2.4 V vs. Li/Li^+ after 5 days then stably sustaining for up to 10 days whereas DME single electrolyte showed a swift decrease of OCV to ~2.1 V vs. Li/Li^+ during a few hours. This rapid decrease of OCV may result from internal shuttling with low viscosity and high lithium polysulfides solubility of DME, in which lithium polysulfides can be formed by sulfur reaction with lithium-ion [28] and can corrode lithium anode. Unlike DME, the OCV with PP13-TFSI/DME is similar as the one with PP13-TFSI only after 10 days. The depressed internal shuttle process of Li–S cells with PP13-TFSI/DME could be further confirmed by the negligible perturbation of cell performance with different rest times. The rest times were programed as 1) 1 min after discharge and 2 min after charge for the first 40 cycles, 2) 10 min after each discharge and charge for the next 20 cycles, and 3) 30 min after each step for the last 40 cycles. Fig. 11a presents the cyclic performance and Coulombic efficiency of the rest time-programed Li–S cell at 1 C of a current rate on 100 cycles. There is no significant capacity fading even with 30 min of the rest time. Representative discharge-rest–charge-rest curves as shown in Fig. 11b also demonstrate negligible deterioration of discharge and charge potentials after the rest.

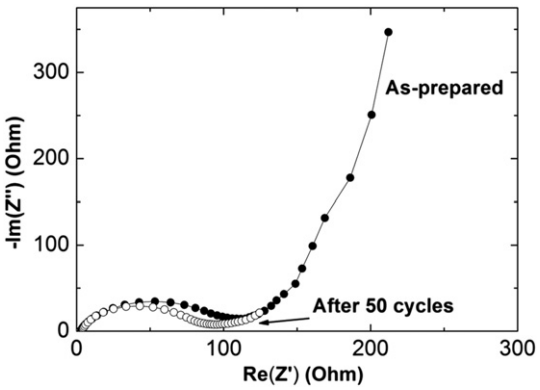

Fig. 9. Electrochemical impedance spectra of Li–S cells as-prepared and after 50 cycles at 0.4 C with 1 M of LiTFSI in PP13-TFSI/DME (2/1, v/v).

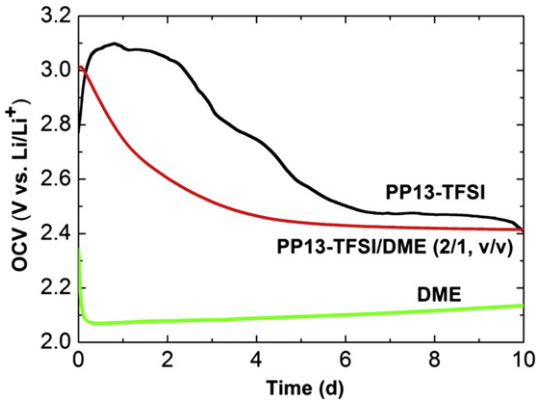

Fig. 10. The change of OCVs of Li–S cells with 1 M of LiTFSI in DME, PP13-TFSI, and PP13-TFSI/DME (2/1, v/v) electrolytes.

3.4. Improved electrochemical performance of Li–S cells

The capacity fading at slow rates in Fig. 7a is mostly attributed to the internal shuttle process as well as the loss of active material and electrical contact from dissolution of bare and weakly bound S particles from the S/KB electrode. Annealing S/KB in a flow Ar gas at a temperature slightly above the melting point of sulfur, the bare sulfur can either be sublimed or trapped within the pores of the KB carbon. This results in the creation of strong adhesive-contact of sulfur with KB carbon and decreased S content (~25 wt%). Li–S cells using these annealed S/KB electrodes demonstrated improved discharge capacity (~1000 mA h g^{-1} at 0.2 C on the first cycle) and capacity retention (~90% capacity retention after 50 cycles) as shown in Fig. 12.

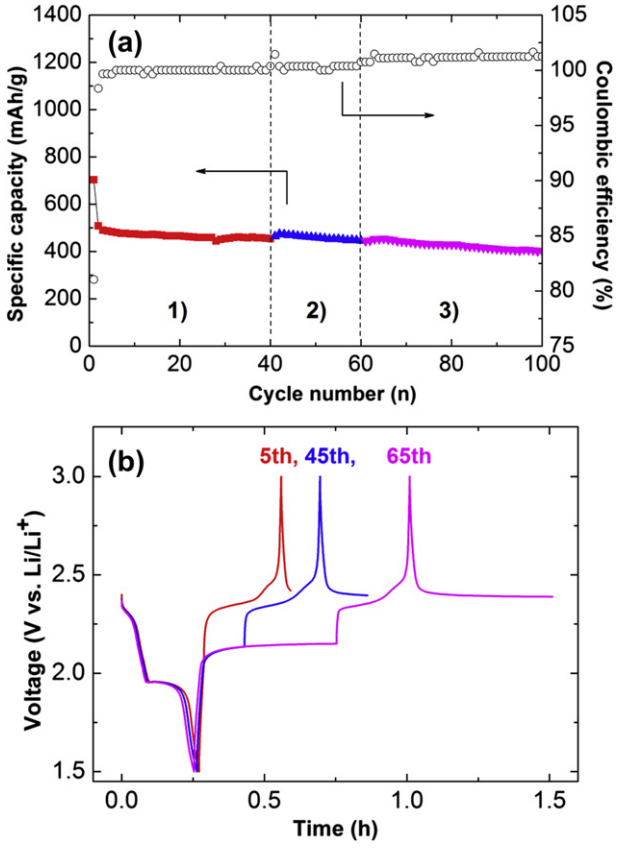

Fig. 11. Rest time-driven Li–S cell performance using 1 M of LiTFSI in PP13-TFSI/DME (2/1, v/v) at 1 C of current rate, programed as (1) 1 min of the rest after discharge and 2 min of rest after charge for the first 40 cycles, (2) 10 min of the rest after each discharge and charge for the next 20 cycles, and (3) 30 min of the rest after each step for the last 40 cycles. (a) Cyclic performance and Coulombic efficiency up to 100 cycles. (b) Representative discharge-rest–charge-rest curves of 5, 45, and 65th of cycles.

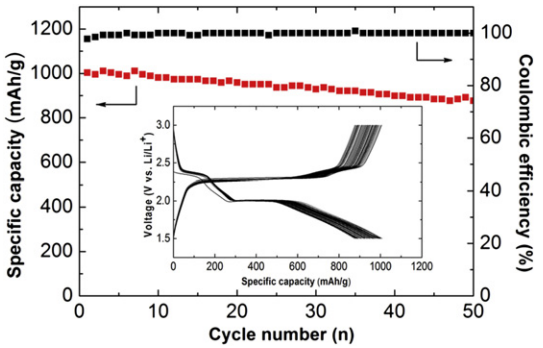

Fig. 12. Cyclic performance of Li–S cells from annealed S/KB electrode with 1 M of LiTFSI in PP13-TFSI/DME (2/1, v/v) at 0.2 C for 50 cycles. The inset is the discharge/charge profiles.

4. Conclusions

In summary, we designed a RTIL-based organic electrolyte for high performance rechargeable Li–S batteries. Engineering of the physicochemical properties of the electrolyte by using high lithium polysulfide solubility of organic solvent and high viscosity of RTIL provided superior specific capacity, Coulombic efficiency and cycling stability. We expect to achieve higher performance for Li–S cells by applying this promising electrolyte to cells fabricated with elaborated cathode structures [4–10], providing an opportunity to further advance Li–S batteries.

Acknowledgments

This work was financially supported by RIKEN Advanced Science Institute (ASI) and Fund for Seeds of Collaborative Research.

References

[1] H.S. Ryu, H.J. Ahn, K.W. Kim, J.H. Ahn, J.Y. Lee, J. Power Sources 153 (2006) 360–364.
[2] X. Ji, S. Evers, R. Black, L.F. Nazar, Nat. Commun. 2 (2011) 325.
[3] P.G. Bruce, S.A. Freunberger, L.J. Hardwick, J.M. Tarascon, Nat. Mater. 11 (2012) 19–29.
[4] J. Schuster, G. He, B. Mandlmeier, T. Yim, K.T. Lee, T. Bein, L.F. Nazar, Angew. Chem. Int. Ed. 51 (2012) 3591–3595.
[5] J. Wang, J. Yang, J. Xie, N. Xu, Adv. Mater. 14 (2002) 963–965.
[6] X. Ji, K.T. Lee, L.F. Nazar, Nat. Mater. 8 (2009) 500–506.
[7] H. Wang, Y. Yang, Y. Liang, J.T. Robinson, Y. Li, A. Jackson, Y. Cui, H. Dai, Nano Lett. 11 (2011) 2644–2647.
[8] F. Wu, J. Chen, R. Chen, S. Wu, L. Li, S. Chen, T. Zhao, J. Phys. Chem. C 115 (2011) 6057–6063.
[9] B. Zhang, X. Qin, G.R. Li, X.P. Gao, Energy Environ. Sci. 3 (2010) 1531–1537.
[10] G. Zheng, Y. Yang, J.J. Cha, S.S. Hong, Y. Cui, Nano Lett. 11 (2011) 4462–4467.
[11] Y. Yang, M.T. McDowell, A. Jackson, J.J. Cha, S.S. Hong, Y. Cui, Nano Lett. 10 (2010) 1486–1491.
[12] L.X. Yuan, J.K. Feng, X.P. Ai, Y.L. Cao, S.L. Chen, H.X. Yang, Electrochem. Commun. 8 (2006) 610–614.
[13] S. Kim, Y. Jung, S.J. Park, J. Power Sources 152 (2005) 272–277.
[14] J.W. Choi, J.K. Kim, G. Cheruvally, J.H. Ahn, H.J. Ahn, K.W. Kim, Electrochim. Acta 52 (2007) 2075–2082.
[15] N. Tachikawa, K. Yamauchi, E. Takashima, J.W. Park, K. Dokko, M. Watanabe, Chem. Commun. 47 (2011) 8157–8159.
[16] J. Shim, K.A. Striebel, E.J. Cairns, J. Electrochem. Soc. 149 (2002) A1321–A1325.
[17] S. Kim, Y. Jung, H.S. Lim, Electrochim. Acta 50 (2004) 889–892.
[18] J. Hassoun, B. Scrosati, Angew. Chem. Int. Ed. 49 (2010) 2371–2374.
[19] J.H. Shin, E.J. Cairns, J. Electrochem. Soc. 155 (2008) A368–A373.

[20] J.H. Shin, E.J. Cairns, J. Power Sources 177 (2008) 537–545.
[21] Y. Mikhaylik, I. Kovalev, R. Schock, K. Kumaresan, J. Xu, J. Affinito, ECS Trans. 25 (2010) 23–34.
[22] E. Peled, Y. Sternberg, A. Gorenshtein, Y. Lavi, J. Electrochem. Soc. 136 (1989) 1621–1625.
[23] D. Aurbach, O. Youngman, P. Dan, Electrochim. Acta 35 (1990) 639–655.
[24] H. Sakaebe, H. Matsumoto, Electrochem. Commun. 5 (2003) 594–598.
[25] J. Nelson, S. Misra, Y. Yang, A. Jackson, Y. Liu, H. Wang, H. Dai, J.C. Andrews, Y. Cui, M.F. Toney, J. Am. Chem. Soc. 134 (2012) 6337–6343.
[26] K. Ueno, H. Tokuda, M. Watanabe, Phys. Chem. Chem. Phys. 12 (2010) 1649–1658.
[27] P.C. Howlett, N. Brack, A.F. Hollenkamp, M. Forsyth, D.R. MacFarlane, J. Electrochem. Soc. 153 (2006) A595–A606.
[28] H.S. Ryu, H.J. Ahn, K.W. Kim, J.H. Ahn, J.Y. Lee, E.J. Cairns, J. Power Sources 140 (2005) 365–369.